HHS Public Access

Author manuscript

Xenotransplantation. Author manuscript; available in PMC 2018 September 01.

Published in final edited form as:

Xenotransplantation. 2017 September ; 24(5): . doi:10.1111/xen.12318.

Aldehyde dehydrogenase 1a1 (*Aldh1a1*) regulates energy metabolism in adipocytes from different species

Kefeng Yang[1,2], **Christopher Adin**[3], **Qiwen Shen**[1], **L. James Lee**[4], **Lianbo Yu**[5], **Paolo Fadda**[6], **Arpad Samogyi**[7], **Kathleen Ham**[8], **Chen Gilor**[9,#], and **Ouliana Ziouzenkova**[1,*,#]

[1]Department of Human Sciences, The Ohio State University, Columbus, Ohio, 43210, USA

[2]Department of Nutrition, School of Medical, Shanghai Jiao Tong University, Shanghai, China. 200025

[3]Department of Clinical Sciences, College of Veterinary Medicine, North Carolina State University, Raleigh, NC 27607, USA

[4]Department of Chemical and Biomolecular Engineering, The Ohio State University, Columbus, Ohio, 43210, USA

[5]Department of Statistics, The Ohio State University College of Medicine, Columbus, OH 43210, USA

[6]Genomics Shared Resource, Comprehensive Cancer Center, The Ohio State University, Columbus, Ohio 43210, USA

[7]Mass Spectrometry and Proteomics Facility, The Ohio State University, Columbus, OH, 43210

[8]Department of Veterinary Clinical Sciences, The Ohio State University, Columbus, OH, 43210

[9]Department of Medicine and Epidemiology, School of Veterinary Medicine, University of California, Davis. One Shields Ave, Davis, California, 95616, USA

Abstract

Background—Survival and longevity of xenotransplants depend on immune function and ability to integrate energy metabolism between cells from different species. However, mechanisms for inter-species crosstalk in energy metabolism are not well understood. White adipose tissue stores energy and is capable of mobilization and dissipation of energy as heat (thermogenesis) by adipocytes expressing uncoupling protein 1 (*Ucp1*). Both pathways are under the control of vitamin A metabolizing enzymes. Deficient retinoic acid production in *aldehyde dehydrogenase 1 family fember A1* (*Aldh1a1*) knock out adipocytes (KO) inhibits adipogenesis and increase thermogenesis. Here we test the role *Aldh1a1* in regulation of lipid metabolism in xenocultures.

[*]**To whom correspondence should be addressed:** Ouliana Ziouzenkova, PhD, 1787 Neil Avenue, 331A Campbell Hall; Columbus, OH 43210, ziouzenkova.1@osu.edu; Telephone: 001 614 292 5034; Fax: 001 614 292 8880.

[#]These laboratories contributed equally to this work

DR. CHEN GILOR (Orcid ID : 0000-0003-0393-4135)

DR. OULIANA ZIOUZENKOVA (Orcid ID : 0000-0003-2449-2591)

CONFLICT OF INTERESTS

The authors declare that they have no conflicts of interests.

Methods—Murine wide type (WT) and KO preadipocytes were encapsulated into a poly-L-lysine polymer that allows exchange of humoral factors <32kD via nanopores. Encapsulated murine adipocytes were co-incubated with primary differentiated canine adipocytes. Then, expression of adipogenic and thermogenic genes in differentiated canine adipocytes were detected by real-time polymerase chain reaction (PCR). The regulatory factors in WT and KO cells were identified by comparison of secretome using proteomics and in transcriptome by gene microarray.

Results—Co-culture of encapsulated mouse KO vs. WT adipocytes increased expression of peroxisome proliferator-activated receptor gamma (*Pparg*), but reduced expression of its target genes *fatty acid binding protein 4* (*Fabp4*), and adipose triglyceride lipase (*Atgl*) in canine adipocytes, suggesting inhibition of PPARγ activation. Co-culture with KO adipocytes also induced expression of *Ucp1* in canine adipocytes compared to expression with WT adipocytes. Cumulatively, murine KO compared to WT adipocytes decreased lipid accumulation in canine adipocytes. Comparative proteomics revealed significantly higher levels of vitamin A carriers, retinol binding protein 4 (RBP4) and lipokalin 2 (LCN2) in KO vs WT adipocytes.

Conclusion—Our data demonstrate the functional exchange of regulatory factors between adipocytes from different species for regulation of energy balance. RBP4 and LCN2 appear to be involved in the transport of retinoids for regulation of lipid accumulation and thermogenesis in xenocultures. While the rarity of thermogenic adipocytes in humans and dogs precludes their use for autologous transplantation, our study demonstrates that xenotransplantation of engineered cells could be a potential solution for reduction of obesity in dogs and a strategy for translation to patients.

Keywords

energy balance; obesity; NGAL; adipogenesis; vitamin A; transplantation; brown; beige; bright adipocytes; xenocultures

INTRODUCTION

Xenotransplantation of organs[1], specific cell populations[2, 3], and genetically engineered cells[4] continue to be investigated to address shortage of donor organs and for treatment of genetic, autoimmune, and degenerative diseases[5]. The survival and longevity of xenografts depends on interaction with the host immune system[6] as well as an ability to integrate into the host's metabolism and energy pathways. Three decades of research led to considerable progress in identification of hallmarks and mechanisms leading to immune rejection[1, 7]. Together these efforts resulted in a considerable improvement in xenograft survival[8–10]. The importance of energy pathways was reveled in context of cancer xenografts in immunosuppressed mice[11, 12]. Energy exchange between different species is also the basis for xenografts' longevity; however, mechanisms for crosstalk establishing energy homeostasis between cells from different species remain understudied.

Studies demonstrate functional survival of xenografts encapsulated into alginate-polylysine polymers (APP) for production of catecholamines[13] or insulin[14]. The longevity of xenotransplanted cells in monkeys was nine months[13], while insulin-producing encapsulated xenotransplants survived for 9.5 years in a human patient[15]. These experiments highlight

humoral factors as key regulators of energy metabolism between host and donor cells, because the small pore size in APP polymers limits influx and efflux of molecules larger than 32kD[16]. However, the identification of these regulatory molecules is challenging in vivo. Insulin has been established as a chief pathway regulating glucose metabolism. Nevertheless, recent studies highlight that endocrine regulation by adipose tissue is similarly crucial for energy homeostasis[17, 18]. Adipokine leptin can efficiently rescue glucose intolerance in the absence of insulin in animal models of type 1 diabetes[18]. Even sub-physiologic levels of leptin produced in encapsulated adipocytes can rescue glucose intolerance in mouse models of type 2 diabetes without influencing insulin levels[19]. In xenocultures, the incompatibility between protein hormones and receptors is expected to limit efficacy of protein-dependent signaling[20]. In contrast, bioactive lipids are conserved signaling mediators that could gain an increasing importance in integration of energy metabolism between cells from different species.

Vitamin A-derived bioactive metabolites, including retinol, retinaldehyde (or retinal, Rald), and retinoic acid, regulate all aspects of adipocyte biology in different species, including differentiation, energy storage, and energy dissipation[21]. Vitamin A is a generic term for many molecules, primarily, all-*trans* retinol and its retinyl esters. Each of these metabolites act via different mechanisms in the regulation of metabolism[22]. Adipose tissue is the second largest store for vitamin A after the liver[21]. Retinoic acid is the principal ligand for retinoic acid receptor and retinoid X receptor (9-*cis* retinoic acid isoform). Retinoic acid also indirectly activates zinc-finger protein 423 (ZFP423) and PPARγ[23], a master regulator of transcription during adipocyte differentiation[22, 24]. In contrast, Rald, suppress PPARγ activation and adipogenesis[25]. In addition, Rald up-regulates ATGL increasing lipolysis and thermogenesis in adipocytes[26]. Retinol can also suppresses adipogenesis[27] when bound with its principal binding protein RBP4[28]. Among multiple enzymes catalyzing reactions with vitamin A metabolites[29], ALDHA1 is the major enzyme converting Rald to retinoic acid in mouse adipocytes[23]. *Aldh1a1*$^{-/-}$ mice resist obesity because of the increased levels of lipolysis and thermogenesis in visceral adipose tissue[16, 26]. Our laboratory has discovered evidence of the contribution of ALDHA1 to regulation of energy homeostasis in an engrafted mouse model[16]. In this model, WT obese mice were treated by engraftment of *Aldh1a1*$^{-/-}$ or WT adipocytes that were encapsulated in APP to avoid immune rejection. The humoral mediators secreted from *Aldh1a1*$^{-/-}$ but not from WT adipocytes, reduced lipid accumulation and increased thermogenesis and metabolic rate in host WT obese mice. These changes may be of therapeutic merit for treatment of obesity in animals having small amount of brown thermogenic adipocytes in adulthood, such as dogs[30] and humans[31]. However, it remains unknown if humoral mediators released from mouse *Aldh1a1*$^{-/-}$ adipocytes are compatible with signaling pathways in these organisms.

Here we report a model for testing of humoral interactions regulating lipid metabolism in xenocultures of canine and mouse adipocytes. We hypothesized that xenogeneic *Aldh1a1*$^{-/-}$ mouse adipocytes would inhibit adipogenesis in canine adipocytes when these cells were co-cultured.

METHODS

Informed owner consent was obtained from clients authorizing the use of discarded tissues for the research.

Chemicals and Reagents

Chemicals and reagents were purchased from Sigma-Aldrich (St. Louis, MO) and cell culture media from Invitrogen Thermo Fischer Scientific, Minneapolis, Minnesota, USA) unless otherwise noted.

Canine adipose stromal cells (ASC)

Canine adipose tissue batches were obtained from healthy dogs admitted to the Ohio State University College of Veterinary Medicine for elective abdominal surgery unrelated to the study. Adipose tissue was excised during routine surgery and was intended to be discarded. Informed owner consent was obtained to use these excised adipose tissues that were considered medical waste. Adipose tissues from two dogs were used: a four-year old female mastiff dog and a one-year old female German shepherd dog. Adipocytes were isolated using a modification of previously described protocols[26, 32]. Briefly, approximately 5g of falciform fat pad was excised and then washed with sterile PBS. The fat was minced with a sterile blade in a P100 petri dish. 5ml of collagenase stock solution (1g collagenase type I (cat # 17100-017), 7.5% BSA 26.7ml, 1M HEPES 2.5ml, add DMEM to 100ml) was added to 45ml of DMEM to make a working solution. Minced tissue was incubated with the collagenase working solution in a 50ml tub at 37°C on a shaker for one hour, before being filtered and centrifuged at 2300rpm for 5 min. The pellet was homogenized by pipetting with DMEM, centrigued, then re-homogenized in 25ml of DMEM before purification using a 100μm cell strainer (BD Falcon). ASC were cultured in DMEM containing 20% FBS and passaged three times.

Differentiation—Adipocyte differentiation was performed as previously described, with some modifications[26]. Briefly, canine ASC were grown to confluency before differentiation in adipogenic differentiation medium I and II. Adipogenic differentiation medium I contained 20% of heat inactivated FBS, 10 μg/mL insulin, 10 μg/mL 3-isobutyl-1-methyl xanthine, and 1μM dexamethasone with or without rosiglitazone (BRL 49653, ALX-350-125-M025, Enzo Life Sciences, Farmingdale, NY). Differentiation medium II contained 20% FBS and 10 μg/mL insulin. Culture medium was replaced by adipogenic differentiation medium I at day 0, then differentiation medium II was added every 48h for 14 days for canine adipocytes.

Mouse cell cultures

Derivation, immortalization, and characterization of WT and *Aldh1a1*$^{-/-}$ preadipocytes was described previously[16], as was a detailed cell encapsulation protocol[33]. Briefly, the cells (2×10^6 cells/ml) were suspended in 2% sodium alginate solution (Sigma, St. Louis, MO, MW 12,000–80,000 g/mol, 100–300 cps Brookfield viscosity). This suspension was extruded through a needle (23 gauge 0.337-mm) into a 100 mM $CaCl_2$ solution, using an encapsulation unit (Nisco Engineering AG, Switzerland) at 5.4 kV to form calcium alginate

gel beads. The gel beads with cells were solidified in 100 mM $CaCl_2$ for 20 min, and formed alginate-poly-L-lysine membrane in 0.05% (w/v) poly-L-lysine (MW 20,700, Sigma, St. Louis, MO). The alginate core was liquefied in 50 mM sodium citrate. Encapsulated preadipocytes were floating in DMEM containing 10% CS for at least 1 week to identify and remove ruptured capsules. Only intact capsules were used for co-cultures with canine adipocytes.

Co-culture of ASC with microcapsules

Canine adipocytes were cultured in 6-well plates until confluent. Then microcapsules containing WT or *Aldh1a1*$^{-/-}$ (KO) preadipocytes were transferred into the 6-well plates to achieve a monolayer of 102 microcapsules/cm^2. Xenocultures were differentiated in differentiation medium I and II for 14 days.

mRNA analysis

Q-PCR—Total mRNA purified from canine adipocytes according to the manufacturer's instructions (Qiagen, Germantown, MD). RNA integrity was analyzed using the Agilent 2100 Bioanalyzer (Agilent Technologies, Santa Clara, CA). mRNA was quantified using 7900HT Fast Real-Time PCR System and TaqMan fluorogenic detection system (Applied Biosystems/ThermoFisher). The *Ucp1* (Cf02622090_m1), *LOC479623* (Cf02644082_m1), *Pparg* (Cf02625640_m1), *Atgl* (*PNPLA2* Cf0260386_g1), *Fabp4* (AIVI5UH) validated primers were also purchased from ThermoFisher. Comparative real-time PCR was performed in triplicate, including no-template controls. Expression was calculated using the comparative Ct method normalized to the TATA box binding protein (TBP, Cf02637234_m1).

Transcriptome analysis

A 100ng aliquot of total RNA was linearly amplified. Then, 5.5μg of cDNA was labeled and fragmented using the GeneChip WT PLUS reagent kit (Affymetrix Santa Clara, CA) following the manufacturer's instructions. Labeled cDNA targets were hybridized to Affymetrix GeneChip Mouse Gene ST 2.0 arrays for 16 h at 45°C rotating at 60rpm. The arrays were washed and stained using a Fluidics Station 450 and scanned using a GeneChip Scanner 3000. Signal intensities were quantified by Affymetrix Expression Console version 1.3.1. Background correction and quantile normalization were performed to adjust for technical bias, and probe-set expression levels were calculated by the RMA method. After filtering above noise cutoff, there are 9,528 probe-sets that were tested by linear model. A variance smoothing method with fully moderated t-statistic was employed for this study and was adjusted by controlling the mean number of false positives. With a combined cutoff of 2-fold change and p-value of 0.0001 (controlling 1 false positive over all probe-sets), we declared 500 probe-sets as differential gene expression between KO and WT preadipocytes. GEO file: 'QS wild type and Aldh1a1 KO preadipocytes 2015'.

Oil Red O staining

Oil Red O staining was performed in canine adipocytes according to the manufacturer's instructions (MAK194, Sigma-Aldrich). Briefly, cells were washed in PBS and then fixed in

10% buffered formalin for 30 min at room temperature. Fixed cells were then rinsed with DI water and 60% isopropanol. A stock solution of 0.5% Oil Red O in isopropanol (w/v) was diluted 60:40 in water and added to fixed cells for 5 min at room temperature. Cell were thenrinsed with DI water. Hematoxylin (2mL/well) was added and incubated for 1 minute. After an additional 1 minute incubation time, the hematoxylin was removed and each well was rinsed with DI water. Lipids appear red and nuclei appear blue after using this staining protocol.

Proteomic 2-D Fluorescence Difference Gel Electrophoresis (DIGE)

Confluent WT and KO adipocytes were differentiated for 4 days. The secretome (10mL/genotype, n=3 per condition) was collected from these cells after 24 h incubation in medium containing 1% FBS. Proteins from the secretome were filtered using Ultracel 50k Ampicon Ultra centrifugal filters (EMD Millipore UFC905024, Cole-Parmer (Ct Vernon Hills, IL, USA) to remove molecules >50 kD. Proteins from the WT and KO secretome (equal volume) were precipitated with 10% trichloroacetic acid and used for DIGE (GE Healthcare, Buckinghamshire, UK) as previously described[26]. Samples were labeled with DIGE fluor minimal-label dyes and focused on 18 cm pH 4–7 Immobiline strips using an IPGphor II IEF. After SDS-PAGE, individual gels were spot mapped using an internal standard. Independent *t*-tests were used to compare spots between WT and *Aldh1a1*$^{-/-}$ groups in males and females. The criteria for performing MS was a >1.5 fold change in expression of proteins in at least 3 of the 4 gels. When significant differences were detected ($P<0.05$), those spots were cored from preparative gels (Ettan workstation) and identified using a LTQ mass spectrometer (MS) detector.

LTQ—Capillary-liquid chromatography-nanospray tandem mass spectrometry (Nano-LC/MS/MS) was performed on a Thermo Finnigan LTQ mass spectrometer equipped with a nanospray source operated in positive ion mode. The LC system was an UltiMate™ Plus system from LC-Packings A Dionex Co (Sunnyvale, CA) with a Famos autosampler and Switchos column switcher. The solvent A was water containing 50 mM acetic acid and the solvent B was acetonitrile. Five microliters of each sample was first injected on to the trapping column (LC-Packings A Dionex Co, Sunnyvale, CA), and washed with 50 mM acetic acid. The injector port was switched to inject and the peptides were eluted off onto the column of the trap. A 5 cm 75 μm ID ProteoPep II C18 column (New Objective, Inc. Woburn, MA) packed directly in the nanospray tip was used for chromatographic separations. Peptides were eluted directly off the column into the LTQ system using a gradient of 2–80%B over 50 minutes, with a flow rate of 300 μl/min. The total run time was 60 minutes. The MS/MS was acquired according to standard conditions established in the lab. Briefly, a nanospray source operated with a spray voltage of 3 KV and a capillary temperature of 200PoPC was used. The scan sequence of the mass spectrometer was based on the TopTen™ method; the analysis was programmed for a full scan recorded between 350 – 2000 Da, and a MS/MS scan to generate product ion spectra to determine amino acid sequence in consecutive instrument scans of the ten most abundant peaks in the spectrum. The CID fragmentation energy was set to 35%. Dynamic exclusion was enabled with a repeat count of 30 s, exclusion duration of 350 s and a low mass width of 0.5 and high mass width of 1.50 Da.

Bioinformatics—Sequence information from the MS/MS data was processed by converting the raw data files into mascot generic files (.mgf) using MS Convert (ProteoWizard). The resulting mgf files were searched against mouse proteins in the Swiss-Prot database (16,702 sequences) using Mascot Daemon by Matrix Science version 2.2.1 (Boston, MA). The mass accuracy of the precursor ions was set to 1.8 Da given that the data was acquired on an ion trap mass analyzer and the fragment mass accuracy was set to 0.8 Da. Considered modifications were methionine oxidation, deamidation (variable) and carbamidomethyl cysteine (fixed). Two missed cleavages for the enzyme were permitted. Peptides with a score less than 20 were filtered and proteins identified required bold red peptides. Protein identifications were checked manually and proteins with a Mascot score of 100 or higher with a minimum of two unique peptides from one protein having a -β or -γ ion sequence tag of five residues or better were accepted. Principal component analysis (PCA) was performed using Progenesis QI software (Nonlinear Dynamics Durham, NC).

Statistical analysis

Data are shown as mean±SD for experiments that were performed at least in triplicate. Group comparisons were performed using one-way ANOVA followed by Tukey's post hoc test unless otherwise indicated. Significance level was set at an alpha = 0.05 unless otherwise noted.

RESULTS

Canine primary ASC differentiate into lipogenic adipocytes in vitro

Canine white adipocytes, which have low levels of lipolysis and thermogenesis[30, 34], were selected as host adipocytes. First, we validated differentiation of canine adipocytes using conventional differentiation protocol and established markers of differentiation *Pparg*, a master regulator of adipogenesis and its target genes *Fabp4* and *Atgl* (*Pnpla2*). We showed that 14 days of differentiation results in the significantly higher expression of *Pparg, Fabp4*, and *Atgl* compared to non-differentiated cells (Figure 1A-C). In the presence of PPARγ ligand BRL-49653 (BRL), the expression of target genes *Fabp4* and *Atgl* was further increased (4878% and 1093%, respectively compared to non-differentiated control) consistent with activation of PPARγ. In agreement with previous findings[34], differentiated canine adipocytes expressed low levels of thermogenic marker *Ucp1* in the presence or absence of BRL (3.38% *vs.* 100% in non-differentiated cells, Figure 1D). The canine homolog for mitochondrial cytochrome oxidase IV (*LOC479623*) expression was moderately increased in canine adipocytes compared to non-differentiated cells (Figure 1E). This response was independent of BRL stimulation consistent with published data in visceral adipose tissue[35]. Together, these standard expression studies validate differentiation in canine adipocytes.

Mouse adipocytes' effect on adipogenesis in canine adipocytes depends on *Aldh1a1*

We described KO and WT preadipocytes line derivation and properties in our previous work[16, 23, 26], where we demonstrate increased expression of UCP1 and ATGL protein as well as lower expression of *Fabp4* and 70% decreased production in retinoic acid in KO compared to WT adipocytes. To identify humoral signaling factors in xenocultures, we

encapsulated mouse WT and KO adipocytes into APP microcapsules that allow exchange of molecules <32 kD. We compared the effect of encapsulated WT and KO preadipocytes on canine adipogenesis (Figure 2 A). We showed that 14 days of differentiation results in significantly higher expression of *Pparg* in canine adipocytes treated with KO when compared to WT adipocyte microcapsules (500.8% vs.100%, Figure 2B). However, the expression of PPARγ target genes *Fabp4* and *Atgl* was reduced (80.3% and 25.5%, respectively vs 100% in WT adipocytes, Figure 2C, D) in canine adipocytes suggesting decreased activity of PPARγ. In contrast, canine adipocytes incubated with encapsulated KO adipocytes expressed 913.5% higher levels of *Ucp1* than those incubated with WT adipocytes (Figure 2E). The cytochrome oxidase expression was similar for both stimulations (Figure 2F). Together these changes in genes responsible for energy homeostasis resulted in decreased lipid accumulation in canine adipocytes treated with encapsulated KO than those encapsulated with WT adipocytes (78.7% *vs.* 100%, Figure 3).

Given potential differences in susceptibility to obesity in different dog breeds[36, 37], we stimulated canine adipocytes isolated from a different dog breed, *e.g.* German shepherd *vs.* mastiff (Figure 2 and 3), with encapsulated WT and KO adipocytes. In these canine adipocytes, KO adipocyte microcapsules induced only 118% increase in *Pparg* expression compared to treatment with WT capsules (Figure 4A). Expression of *Fabp4* and *Atgl* were reduced when incubated with KO adipocytes (20.6% and 8.0 %, respectively *vs.* 100% in WT adipocytes, Figure 4B, C), suggesting that PPARγ activity was also decreased in these canine adipocytes. *Ucp1* expression was also induced in the presence of encapsulated KO *vs.* WT adipocytes (3498% *vs.* 100%, Figure 4D). Similarly, the expression of cytochrome oxidase 4 was not different in canine adipocytes stimulated with encapsulated WT and KO adipocytes (Figure 4E). The net effect of stimulation with KO *vs.* WT microcapsulated adipocytes resulted in lipid accumulation (72.5% *vs.* 100%, Figure 5).

Aldh1a1 regulates transport of vitamin A via regulation of RBP4 and LCN2 levels

ALDH1A1 alters intracellular and extracellular concentration of bioactive vitamin A metabolites[23, 25, 38]. However, binding proteins are required for their transport[39]. To identify mediators of energy metabolism in our xenoculture model, we collected the secretome from KO and WT adipocytes and analyzed it using comparative proteomic DIGE analysis (Figure 6A) followed by analysis of variation between proteins by principal component analysis (Figure 6B). Analysis revealed 155 proteins that exhibited an average change of at least 2.5-fold (P<0.05) when comparing KO vs WT samples (Table 1). Among 155 proteins secreted in high abundance from KO vs WT adipocytes, two lipocalins RBP4 and lipocalin-2 (LCN2 or neutrophil gelatinase-associated lipocalin, NGAL) were proteins implicated in retinol transport[28, 40] (Figure C-F). RBP4 levels were markedly higher in KO than in WT secretome (Figure 6C). The increase in RBP4 secretion was linked to the increase in *Rbp4* expression, which was found using transcriptome comparison in KO and WT cells (Figure 6D). LCN2 levels were also significantly higher in secretome from KO when compared to WT adipocytes (Figure 6E). However, *Lcn2* expression was reduced in KO compared to WT adipocytes consistent with its regulation by retinoic acid[40] (Figure 6F).

DISCUSSION

Transplantation of pancreatic β-cells[15], thermogenic[41, 42], fetal[43] and genetically-modified adipocytes[16, 19], and other minor cell populations[2] showed therapeutic promise for treatment of many degenerative disorders including diabetes and obesity. However, systemic and immune effects in vivo limits possibilities to dissect mechanisms for interaction between xenograft and host organism. Here we showed an in vitro model to study crosstalk between canine and murine adipocytes in the absence of systemic effects and immune response. Our study revealed that mouse adipocytes can effectively modify energy metabolism in canine adipocytes. The fundamental energy regulation pathways were regulated by paracrine mechanisms involving exchange between humoral factors through nanopores in the APP microcapsule.

The line of evidence suggests that regulation of energy balance in xenocultures in our study was dependent on lipids, specifically on vitamin A metabolites. The genetic evidence showed that deletion of ALDH1A1 enzyme in mouse adipocytes switches adipogenic programs in canine adipocytes to thermogenic gene expression. The triglyceride storage seen with murine WT adipocytes was reduced in the presence of KO cells, suggesting increased energy expenditure in these cells expressing increased levels of *Ucp1*. The major function of ALDH1A1 is in oxidation of lipid aldehydes into respective acids[38, 44]. Therefore, in the absence of *Aldh1a1* in KO adipocytes, its lipid substrate switches adipogenic programs to thermogenic programs. Rald is a major substrate for ALDH1A1 that is responsible for 70% of retinoic acid in adipocytes[23]. Rald has been shown to inhibit PPARγ activation[25]. Hydroxynonenal is another ALDH1A1 substrate (low affinity), which can also inhibit lipid accumulation[45]. Thus, ALDH1A1 function suggests a lipid-dependent mechanism for regulation of energy homeostasis in xenocultures. Although identification of a particular lipid mediator was beyond the scope of this first study, it is plausible that xenoculture utilized evolutionary-conserved lipid signaling pathways for energy metabolism that can bypass immune recognition systems.

Lipid mediators require carriers to transduce signal in distal canine adipocyte culture. The next supportive finding was based on the presence of elevated levels of two lipocalins, LCN2 and RBP4 in KO secretome compared to WT adipocytes. Lipocalins are a conserved group of proteins[46] transporting lipids[47]. Both LCN2 and RBP4 are responsible for transport of vitamin A metabolites[28, 40]. The major side of LCN2 and RBP4 secretion overlaps with the major storage side of retinol. Although LCN2 and RBP4 are secreted predominantly from liver, adipocytes also express *Lcn2* and *Rbp4* and significantly contribute to the secretion of LCN2[40] and RBP4[48]. Furthermore, vitamin A metabolites control expression and secretion of LCN2[40] and RBP4[40, 49], although these response appear to be different between adipose depots and hepatic tissues. In agreement with retinoic acid-dependent regulation of *Lcn2*, its expression was decreased in KO adipocytes with reduced RA production. However, LCN2 secretion was increased in KO cells in our experiments, similar to the secretions of RBP4 and in agreement with previous reports in KO mice[25]. This increased secretion could be facilitated by retinol[40, 49]. Consistent with this speculation, both RBP4-retinol complex and LCN2 induce UCP1 expression and thermogenesis in adipocytes[27, 40]. In our study, in canine adipocytes retinoid homeostasis in KO adipocytes also was associated with switching

from energy storage to energy dissipation pathways. Multiple factors, including metabolites, microRNA, peptides, could, potentially, regulate energy balance; future work will assess contribution LCN, RBP4, their ligands, and other factors to the regulation of energy metabolism,

This pathway, regulating energy in xenocultures, could shed light on the understanding of mechanisms for transplant rejection. Increased LCN2 levels are a marker of acute transplant rejection in different species[50, 51]. *Lcn2*$^{-/-}$ kidney allografts were protected from rejection in mouse recipients[52]. Remarkably, recombinant apo-LCN2 could effectively rescue kidney allografts from rejection to a similar extent as the immunosuppressant cyclosporine A[52]. Future studies, could investigate the link between vitamin A metabolism, vitamin A transport via LCN2 and energy pathways in donor organs and recipients. In addition, the role of LCN2 in paracrine delivery of vitamin A metabolites in immune cells could also play a crucial role in the immune recognition and rejection response that is known to be regulated by retinoic acid and vitamin A metabolism[53, 54].

The effect of decreased lipid accumulation in canine adipocytes by encapsulated KO xenograft can have important implications for treatment of metabolic diseases, particularly obesity. Dogs and humans have high natal levels of thermogenic brown fat, which is gradually decreased in adulthood rendering them susceptible to obesity and insulin resistance[30, 55, 56]. Obesity is considered to be a modern epidemic influencing 30% of world population[57]. Companion animals, such dogs, cats, and horses have similar obesity epidemics[37, 58]. Obesity increases risk for type 2 diabetes and cardiovascular disease in humans as well as in cats and horses[59, 60]. Given the small number of thermogenic adipocytes in these species, they are not reliable source for autoglogous or allogenic treatment. Development of thermogenic autoglogous engrafts from stem cells is expensive and time-consuming. UCP1 and ATGL represent critical junctions in energy dissipation and energy mobilization, respectively[61, 62]. Thermogenesis and lipolysis are both under control of systemic endocrine and sympathetic nervous tissue response activating β-adrenergic pathways in mice, dogs, and humans[55, 56, 63]. In our study, paracrine mediators from encapsulated KO adipocytes acted autonomously upon induction of *Ucp1* expression in canine adipocytes. Encapsulation in APP should protect KO cells from immune rejection[64]. Therefore, development of encapsulated engineered xenografts of KO adipocytes can present a cost- effective solution for long-lasting treatment of obesity in many species. Stromal vascular cells from adipose tissue are found to have increasingly more application in other diseases, including lupus[65], osteoarthritis[66], neuron regeneration after spine cord injuries[67], and other conditions. The proposed model can potentially be used for both mechanistic studies identifying paracrine interactions as well as adapted for therapeutic purpose.

Acknowledgments

This research was supported by NIH grants R21OD017244 (O.Z., X.L.), the National Center for Research Resources UL1RR025755, UL1TR001070, and NCI P30CA16058 (OSUCCC), and the NIH Roadmap for Medical Research. The content is solely the responsibility of the authors and does not necessarily represent the official views of the National Center for Research Resources or the National Institutes of Health. This research was supported by the Canine Intramural Grant at Ohio State (C.G., C.A., K.Y.,O.Z) as well as, Accelerator Award from Technology and Commercialization office at OSU, and SEED grant from College of Education and Human Ecology at OSU (O.Z). K.Y. also was supported by a fellowship from Chinese Scholarship Council. The project was supported by

Grant UL1TR001070 from the National Center for Advancing Translational Sciences. The content is solely the responsibility of the authors and does not necessarily represent the official views of the National Center for Advancing Translational Sciences.

Abbreviations

ASC	Canine adipose stromal cells
Atgl	Adipose triglyceride lipase
BRL	BRL-49653(Rosiglitazone)
APP	alginate-polylysine polymers
BSA	bovine serum albumin
CID	Collision-induced dissociation
CS	calf serum
DIGE	Difference Gel Electrophoresis
DMEM	Dulbecco's Modified Eagle Medium
Fabp4	Fatty acid binding protein 4
FBS	Fetal bovine serum
HEPES	4-(2-hydroxyethyl)-1-piperazineethanesulfonic acid
IEF	Isoelectric focusing
KO	Knock out
LCN2	Lipokalin 2
LTQ	Linear Trap Quadrupole
MGF	mascot generic files
MS	mass spectrometry
NGAL	Neutrophil gelatinase-associated lipocalin
PBS	Phosphate-buffered saline
PCA	Principal component analysis
PCR	Polymerase chain reaction
Pparg	Peroxisome proliferator-activated receptor gamma
Rald	Retinaldehyde
RBP4	Retinol binding protein 4
SDS-PAGE	Sodium dodecyl sulfate polyacrylamide gel electrophoresis

Ucp1	Uncoupling protein 1
WT	Wide type
Zfp423	zinc-finger protein 423

References

1. Niemann H, Petersen B. The production of multi-transgenic pigs: update and perspectives for xenotransplantation. Transgenic research. 2016; 25:361–374. [PubMed: 26820415]
2. Luca G, Arato I, Mancuso F, Calvitti M, Falabella G, Murdolo G, et al. Xenograft of microencapsulated Sertoli cells restores glucose homeostasis in db/db mice with spontaneous diabetes mellitus. Xenotransplantation. 2016; 23:429–439. [PubMed: 27678013]
3. Pellegrini S, Cantarelli E, Sordi V, Nano R, Piemonti L. The state of the art of islet transplantation and cell therapy in type 1 diabetes. Acta diabetologica. 2016; 53:683–691. [PubMed: 26923700]
4. Ock SA, Lee J, Oh KB, Hwang S, Yun IJ, Ahn C, et al. Molecular immunology profiles of monkeys following xenografting with the islets and heart of alpha-1,3-galactosyltransferase knockout pigs. Xenotransplantation. 2016; 23:357–369. [PubMed: 27511303]
5. Ekser B, Cooper DK, Tector AJ. The need for xenotransplantation as a source of organs and cells for clinical transplantation. International journal of surgery. 2015; 23:199–204. [PubMed: 26188183]
6. Pitkin Z. New Phase of Growth for Xenogeneic-Based Bioartificial Organs. International journal of molecular sciences. 2016; 17
7. van den Heuvel H, Heidt S, Roelen DL, Claas FH. T-cell alloreactivity and transplantation outcome: a budding role for heterologous immunity? Current opinion in organ transplantation. 2015; 20:454–460. [PubMed: 26126194]
8. Shin JS, Kim JM, Kim JS, Min BH, Kim YH, Kim HJ, et al. Long-term control of diabetes in immunosuppressed nonhuman primates (NHP) by the transplantation of adult porcine islets. American journal of transplantation : official journal of the American Society of Transplantation and the American Society of Transplant Surgeons. 2015; 15:2837–2850.
9. Lee HS, Lee JG, Yeom HJ, Chung YS, Kang B, Hurh S, et al. The Introduction of Human Heme Oxygenase-1 and Soluble Tumor Necrosis Factor-alpha Receptor Type I With Human IgG1 Fc in Porcine Islets Prolongs Islet Xenograft Survival in Humanized Mice. American journal of transplantation : official journal of the American Society of Transplantation and the American Society of Transplant Surgeons. 2016; 16:44–57.
10. Tena AA, Sachs DH, Mallard C, Yang YG, Tasaki M, Farkash E, et al. Prolonged Survival of Pig Skin on Baboons After Administration of Pig Cells Expressing Human CD47. Transplantation. 2017; 101:316–321. [PubMed: 27232934]
11. Kubo A, Ohmura M, Wakui M, Harada T, Kajihara S, Ogawa K, et al. Semi-quantitative analyses of metabolic systems of human colon cancer metastatic xenografts in livers of superimmunodeficient NOG mice. Analytical and bioanalytical chemistry. 2011; 400:1895–1904. [PubMed: 21479793]
12. Pollak M. Do cancer cells care if their host is hungry? Cell metabolism. 2009; 9:401–403. [PubMed: 19416708]
13. Xue YL, Wang ZF, Zhong DG, Cui X, Li XJ, Ma XJ, et al. Xenotransplantation of microencapsulated bovine chromaffin cells into hemiparkinsonian monkeys. Artificial cells, blood substitutes, and immobilization biotechnology. 2000; 28:337–345.
14. Elliott RB, Escobar L, Calafiore R, Basta G, Garkavenko O, Vasconcellos A, et al. Transplantation of micro- and macroencapsulated piglet islets into mice and monkeys. Transplantation proceedings. 2005; 37:466–469. [PubMed: 15808678]
15. Elliott RB, Escobar L, Tan PL, Muzina M, Zwain S, Buchanan C. Live encapsulated porcine islets from a type 1 diabetic patient 9.5 yr after xenotransplantation. Xenotransplantation. 2007; 14:157–161. [PubMed: 17381690]

16. Yang F, Zhang X, Maiseyeu A, Mihai G, Yasmeen R, DiSilvestro D, et al. The prolonged survival of fibroblasts with forced lipid catabolism in visceral fat following encapsulation in alginate-poly-L-lysine. Biomaterials. 2012; 33:5638–5649. [PubMed: 22575837]
17. Dodd GT, Decherf S, Loh K, Simonds SE, Wiede F, Balland E, et al. Leptin and insulin act on POMC neurons to promote the browning of white fat. Cell. 2015; 160:88–104. [PubMed: 25594176]
18. Fujikawa T, Berglund ED, Patel VR, Ramadori G, Vianna CR, Vong L, et al. Leptin engages a hypothalamic neurocircuitry to permit survival in the absence of insulin. Cell metabolism. 2013; 18:431–444. [PubMed: 24011077]
19. DiSilvestro DJ, Melgar-Bermudez E, Yasmeen R, Fadda P, Lee LJ, Kalyanasundaram A, et al. Leptin Production by Encapsulated Adipocytes Increases Brown Fat, Decreases Resistin, and Improves Glucose Intolerance in Obese Mice. PloS one. 2016; 11:e0153198. [PubMed: 27055280]
20. Popovic V, Damjanovic S, Dieguez C, Casanueva FF. Leptin and the pituitary. Pituitary. 2001; 4:7–14. [PubMed: 11824510]
21. Jeyakumar SMYR, Reichert B, Ziouzenkova O. Metabolism of vitamin A in white adipose tissue and obesity. Carotenoids and Vitamin A in Translational Medicine. 2013:23–52.
22. Yasmeen R, Jeyakumar SM, Reichert B, Yang F, Ziouzenkova O. The contribution of vitamin A to autocrine regulation of fat depots. Biochimica et biophysica acta. 2012; 1821:190–197. [PubMed: 21704731]
23. Reichert B, Yasmeen R, Jeyakumar SM, Yang F, Thomou T, Alder H, et al. Concerted action of aldehyde dehydrogenases influences depot-specific fat formation. Molecular endocrinology. 2011; 25:799–809. [PubMed: 21436255]
24. Gupta RK, Arany Z, Seale P, Mepani RJ, Ye L, Conroe HM, et al. Transcriptional control of preadipocyte determination by Zfp423. Nature. 2010; 464:619–623. [PubMed: 20200519]
25. Ziouzenkova O, Orasanu G, Sharlach M, Akiyama TE, Berger JP, Viereck J, et al. Retinaldehyde represses adipogenesis and diet-induced obesity. Nature medicine. 2007; 13:695–702.
26. Yasmeen R, Reichert B, Deiuliis J, Yang F, Lynch A, Meyers J, et al. Autocrine function of aldehyde dehydrogenase 1 as a determinant of diet- and sex-specific differences in visceral adiposity. Diabetes. 2013; 62:124–136. [PubMed: 22933113]
27. Muenzner M, Tuvia N, Deutschmann C, Witte N, Tolkachov A, Valai A, et al. Retinol-binding protein 4 and its membrane receptor STRA6 control adipogenesis by regulating cellular retinoid homeostasis and retinoic acid receptor alpha activity. Molecular and cellular biology. 2013; 33:4068–4082. [PubMed: 23959802]
28. Quadro L, Blaner WS, Salchow DJ, Vogel S, Piantedosi R, Gouras P, et al. Impaired retinal function and vitamin A availability in mice lacking retinol-binding protein. The EMBO journal. 1999; 18:4633–4644. [PubMed: 10469643]
29. Kumar S, Sandell LL, Trainor PA, Koentgen F, Duester G. Alcohol and aldehyde dehydrogenases: retinoid metabolic effects in mouse knockout models. Biochimica et biophysica acta. 2012; 1821:198–205. [PubMed: 21515404]
30. Holloway BR, Stribling D, Freeman S, Jamieson L. The thermogenic role of adipose tissue in the dog. International journal of obesity. 1985; 9:423–432. [PubMed: 3007382]
31. Cypess AM, Lehman S, Williams G, Tal I, Rodman D, Goldfine AB, et al. Identification and importance of brown adipose tissue in adult humans. The New England journal of medicine. 2009; 360:1509–1517. [PubMed: 19357406]
32. Kiefer KM, O'Brien TD, Pluhar EG, Conzemius M. Canine adipose-derived stromal cell viability following exposure to synovial fluid from osteoarthritic joints. Veterinary record open. 2015; 2:e000063. [PubMed: 26392889]
33. Xu L, Shen Q, Mao Z, Lee LJ, Ziouzenkova O. Encapsulation Thermogenic Preadipocytes for Transplantation into Adipose Tissue Depots. Journal of visualized experiments : JoVE. 2015:e52806. [PubMed: 26066392]
34. Omachi A, Matsushita Y, Kimura K, Saito M. Role of uncoupling protein 1 in the anti-obesity effect of beta3-adrenergic agonist in the dog. Research in veterinary science. 2008; 85:214–219. [PubMed: 18406437]

35. Distel E, Penot G, Cadoudal T, Balguy I, Durant S, Benelli C. Early induction of a brown-like phenotype by rosiglitazone in the epicardial adipose tissue of fatty Zucker rats. Biochimie. 2012; 94:1660–1667. [PubMed: 22575275]
36. Nishii N, Takasu M, Soe OK, Maeda S, Ohba Y, Inoue-Murayama M, et al. Cloning, expression and investigation for polymorphisms of canine peroxisome proliferator-activated receptors. Comparative biochemistry and physiology. Part B, Biochemistry & molecular biology. 2007; 147:690–697.
37. Switonski M, Mankowska M. Dog obesity--the need for identifying predisposing genetic markers. Research in veterinary science. 2013; 95:831–836. [PubMed: 24034586]
38. Molotkov A, Duester G. Genetic evidence that retinaldehyde dehydrogenase Raldh1 (Aldh1a1) functions downstream of alcohol dehydrogenase Adh1 in metabolism of retinol to retinoic acid. The Journal of biological chemistry. 2003; 278:36085–36090. [PubMed: 12851412]
39. Frey SK, Vogel S. Vitamin A metabolism and adipose tissue biology. Nutrients. 2011; 3:27–39. [PubMed: 22254074]
40. Guo H, Foncea R, O'Byrne SM, Jiang H, Zhang Y, Deis JA, et al. Lipocalin 2, a Regulator of Retinoid Homeostasis and Retinoid-mediated Thermogenic Activation in Adipose Tissue. The Journal of biological chemistry. 2016; 291:11216–11229. [PubMed: 27008859]
41. Tharp KM, Jha AK, Kraiczy J, Yesian A, Karateev G, Sinisi R, et al. Matrix-Assisted Transplantation of Functional Beige Adipose Tissue. Diabetes. 2015; 64:3713–3724. [PubMed: 26293504]
42. Min SY, Kady J, Nam M, Rojas-Rodriguez R, Berkenwald A, Kim JH, et al. Human 'brite/beige' adipocytes develop from capillary networks, and their implantation improves metabolic homeostasis in mice. Nature medicine. 2016; 22:312–318.
43. Garcia B, Francois-Vaughan H, Onikoyi O, Kostadinov S, De Paepe ME, Gruppuso PA, et al. Xenotransplantation of human fetal adipose tissue: a model of in vivo adipose tissue expansion and adipogenesis. Journal of lipid research. 2014; 55:2685–2691. [PubMed: 25193996]
44. Xiao T, Shoeb M, Siddiqui MS, Zhang M, Ramana KV, Srivastava SK, et al. Molecular cloning and oxidative modification of human lens ALDH1A1: implication in impaired detoxification of lipid aldehydes. Journal of toxicology and environmental health. Part A. 2009; 72:577–584. [PubMed: 19296407]
45. Dasuri K, Ebenezer P, Fernandez-Kim SO, Zhang L, Gao Z, Bruce-Keller AJ, et al. Role of physiological levels of 4-hydroxynonenal on adipocyte biology: implications for obesity and metabolic syndrome. Free radical research. 2013; 47:8–19. [PubMed: 23025469]
46. Salier JP. Chromosomal location, exon/intron organization and evolution of lipocalin genes. Biochimica et biophysica acta. 2000; 1482:25–34. [PubMed: 11058744]
47. di Masi A, Trezza V, Leboffe L, Ascenzi P. Human plasma lipocalins and serum albumin: Plasma alternative carriers? Journal of controlled release : official journal of the Controlled Release Society. 2016; 228:191–205. [PubMed: 26951925]
48. Yang Q, Graham TE, Mody N, Preitner F, Peroni OD, Zabolotny JM, et al. Serum retinol binding protein 4 contributes to insulin resistance in obesity and type 2 diabetes. Nature. 2005; 436:356–362. [PubMed: 16034410]
49. Smith JE, Borek C, Goodman DS. Regulation of retinol-binding protein metabolism in cultured rat liver cell lines. Cell. 1978; 15:865–873. [PubMed: 569553]
50. Field M, Lowe D, Cobbold M, Higgins R, Briggs D, Inston N, et al. The use of NGAL and IP-10 in the prediction of early acute rejection in highly sensitized patients following HLA-incompatible renal transplantation. Transplant international : official journal of the European Society for Organ Transplantation. 2014; 27:362–370. [PubMed: 24438378]
51. Wei W, Huang XH, Liang D, Zeng YY, Ma C, Wu YB, et al. A proteomic analysis of transplanted liver in a rat model of chronic rejection. Clinics and research in hepatology and gastroenterology. 2015; 39:340–350. [PubMed: 25468549]
52. Ashraf MI, Schwelberger HG, Brendel KA, Feurle J, Andrassy J, Kotsch K, et al. Exogenous Lipocalin 2 Ameliorates Acute Rejection in a Mouse Model of Renal Transplantation. American journal of transplantation : official journal of the American Society of Transplantation and the American Society of Transplant Surgeons. 2016; 16:808–820.

53. Morales RA, Campos-Mora M, Gajardo T, Perez F, Campos J, Aguillon JC, et al. Retinaldehyde dehydrogenase activity is triggered during allograft rejection and it drives Th1/Th17 cytokine production. Immunobiology. 2015; 220:769–774. [PubMed: 25592248]
54. Moore C, Tejon G, Fuentes C, Hidalgo Y, Bono MR, Maldonado P, et al. Alloreactive regulatory T cells generated with retinoic acid prevent skin allograft rejection. European journal of immunology. 2015; 45:452–463. [PubMed: 25381698]
55. Halpern B, Mancini MC, Halpern A. Brown adipose tissue: what have we learned since its recent identification in human adults. Arquivos brasileiros de endocrinologia e metabologia. 2014; 58:889–899. [PubMed: 25627043]
56. Ashwell M, Stirling D, Freeman S, Holloway BR. Immunological, histological and biochemical assessment of brown adipose tissue activity in neonatal, control and beta-stimulant-treated adult dogs. International journal of obesity. 1987; 11:357–365. [PubMed: 2889691]
57. Ogden CL, Yanovski SZ, Carroll MD, Flegal KM. The epidemiology of obesity. Gastroenterology. 2007; 132:2087–2102. [PubMed: 17498505]
58. Raffan E. The big problem: battling companion animal obesity. The Veterinary record. 2013; 173:287–291. [PubMed: 24077144]
59. Osto M, Lutz TA. Translational value of animal models of obesity-Focus on dogs and cats. European journal of pharmacology. 2015; 759:240–252. [PubMed: 25814247]
60. Johnson PJ, Wiedmeyer CE, LaCarrubba A, Ganjam VK, Messer NTt. Diabetes, insulin resistance, and metabolic syndrome in horses. Journal of diabetes science and technology. 2012; 6:534–540. [PubMed: 22768883]
61. Ahmadian M, Abbott MJ, Tang T, Hudak CS, Kim Y, Bruss M, et al. Desnutrin/ATGL is regulated by AMPK and is required for a brown adipose phenotype. Cell metabolism. 2011; 13:739–748. [PubMed: 21641555]
62. Lass A, Zimmermann R, Oberer M, Zechner R. Lipolysis - a highly regulated multi-enzyme complex mediates the catabolism of cellular fat stores. Progress in lipid research. 2011; 50:14–27. [PubMed: 21087632]
63. Lawrence VJ, Coppack SW. The endocrine function of the fat cell-regulation by the sympathetic nervous system. Hormone and metabolic research = Hormon- und Stoffwechselforschung = Hormones et metabolisme. 2000; 32:453–467. [PubMed: 11246810]
64. Krishnan R, Ko D, Foster CE 3rd, Liu W, Smink AM, de Haan B, et al. Immunological Challenges Facing Translation of Alginate Encapsulated Porcine Islet Xenotransplantation to Human Clinical Trials. Methods in molecular biology. 2017; 1479:305–333. [PubMed: 27738946]
65. Choi EW, Shin IS, Park SY, Park JH, Kim JS, Yoon EJ, et al. Reversal of serologic, immunologic, and histologic dysfunction in mice with systemic lupus erythematosus by long-term serial adipose tissue-derived mesenchymal stem cell transplantation. Arthritis and rheumatism. 2012; 64:243–253. [PubMed: 21904997]
66. Black LL, Gaynor J, Gahring D, Adams C, Aron D, Harman S, et al. Effect of adipose-derived mesenchymal stem and regenerative cells on lameness in dogs with chronic osteoarthritis of the coxofemoral joints: a randomized, double-blinded, multicenter, controlled trial. Veterinary therapeutics : research in applied veterinary medicine. 2007; 8:272–284. [PubMed: 18183546]
67. Forostyak S, Jendelova P, Sykova E. The role of mesenchymal stromal cells in spinal cord injury, regenerative medicine and possible clinical applications. Biochimie. 2013; 95:2257–2270. [PubMed: 23994163]

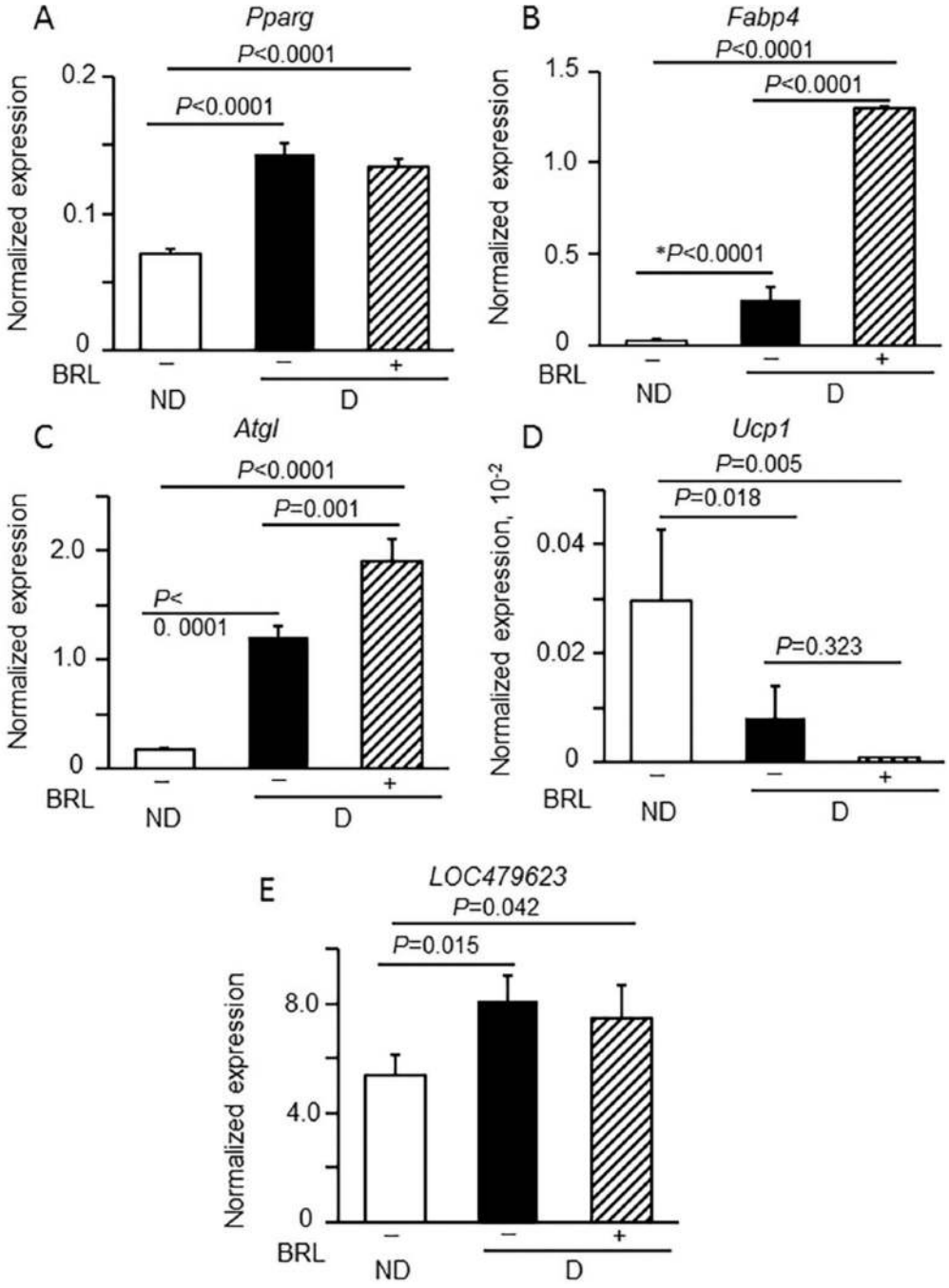

Figure 1. Canine adipocytes express higher levels of differentiation markers *PPARg* and *Fabp4*, and reduced levels of *Ucp1* than non-differentiated ASC

ASC were isolated from falciform adipose depot of a female Mastiff dog and cultured for 3 passages. The resulted primary non-differentiated pre-adipocytes (ND) were differentiated in adipogenic medium (DMI and DM II) with or without 1μM BRL for 14 days (D for Differentiated). RNA expression of *Pparg* (A), *Fabp4* (B), *Atgl* (C), *Ucp1* (D) and *LOC479623* (E) were measured in non-differentiated and differentiated canine adipocytes using Q-PCR assay and TaqMan probes. The values were normalized by TBP and represent the mean ± SD (n=3), one-way ANOVA.

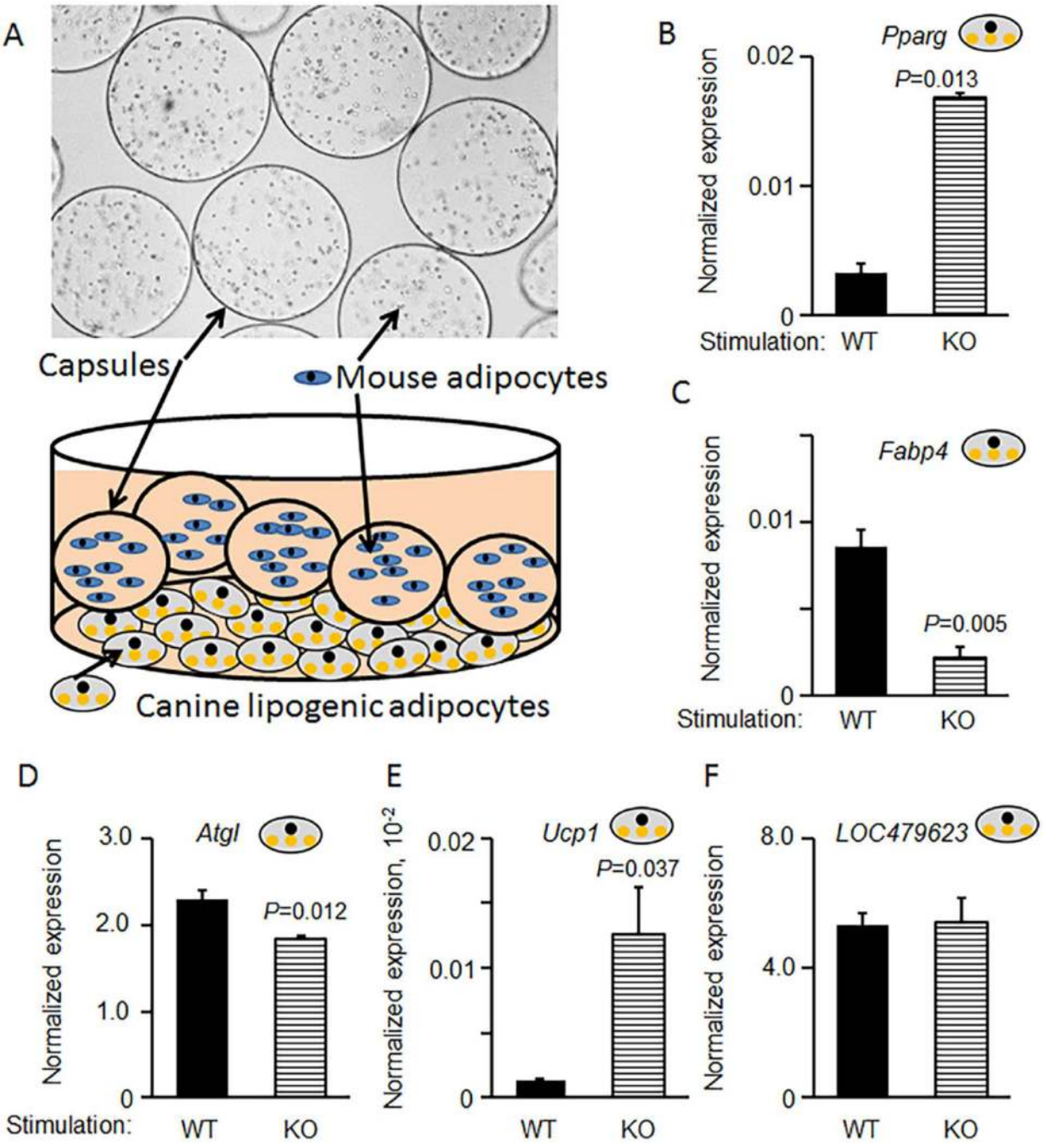

Figure 2. Co-culture of encapsulated WT vs KO murine preadipocytes alter gene expression in canine adipocytes

Schematic presentation of an experiment in which encapsulated murine preadipocytes were co-cultured and differentiated with adherent canine preadipocytes (A). The upper panel shows encapsulated murine preadipocytes floating in media under light microscopy (20x magnification). In schematics, differentiated canine adipocytes were depicted as adherent cells containing yellow lipid droplets. Numerous murine adipocytes (blue ellipses) are floating in the media within microcapsules (circles) Canine preadipocytes (Mastiff dog) were differentiated in adipogenic medium with encapsulated WT or *Aldh1a1*$^{-/-}$ (KO)

preadipocytes for 14 days (B-F). Expression of *Pparg* (B), *Fabp4* (C), *Atgl* (D), *Ucp1* (E) and *LOC479623* (F) were measured by Q-PCR assay TaqMan. The values were normalized by TBP and represent the mean ± SD (n=3), one-way ANOVA.

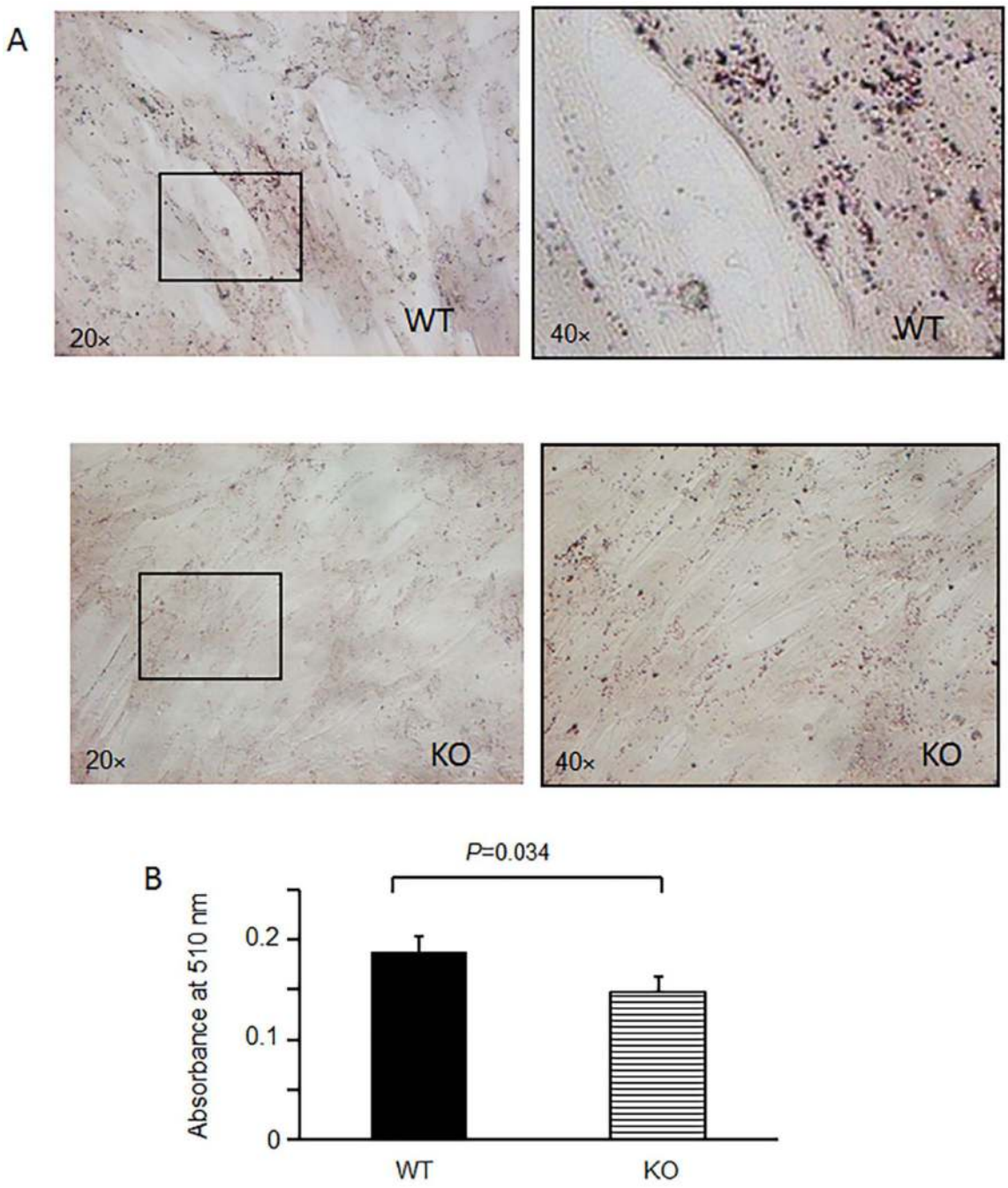

Figure 3. Encapsulated KO cells reduce lipid accumulation in canine adipocytes

Canine preadipocytes from a Mastiff dog were differentiated in adipogenic medium with encapsulated WT (upper panel in A, black bar in B) or KO preadipocytes (lower panel in A, patterned bars in B) for 14 days. Encapsulated WT and KO cells were removed. Neutral lipid accumulation in lipid droplet is shown in differentiated canine adipocytes using Oil Red O staining (A). Left panels showed enlarged (40x magnification) areas (square) in the right panels A. Lipid accumulation was quantified in isopropanol extract from these Oil red

stained canine adipocytes by detecting absorbance of dissolved oil red staining at 510nm (B). Data are shown as mean ± SD (n=3), one-way ANOVA.

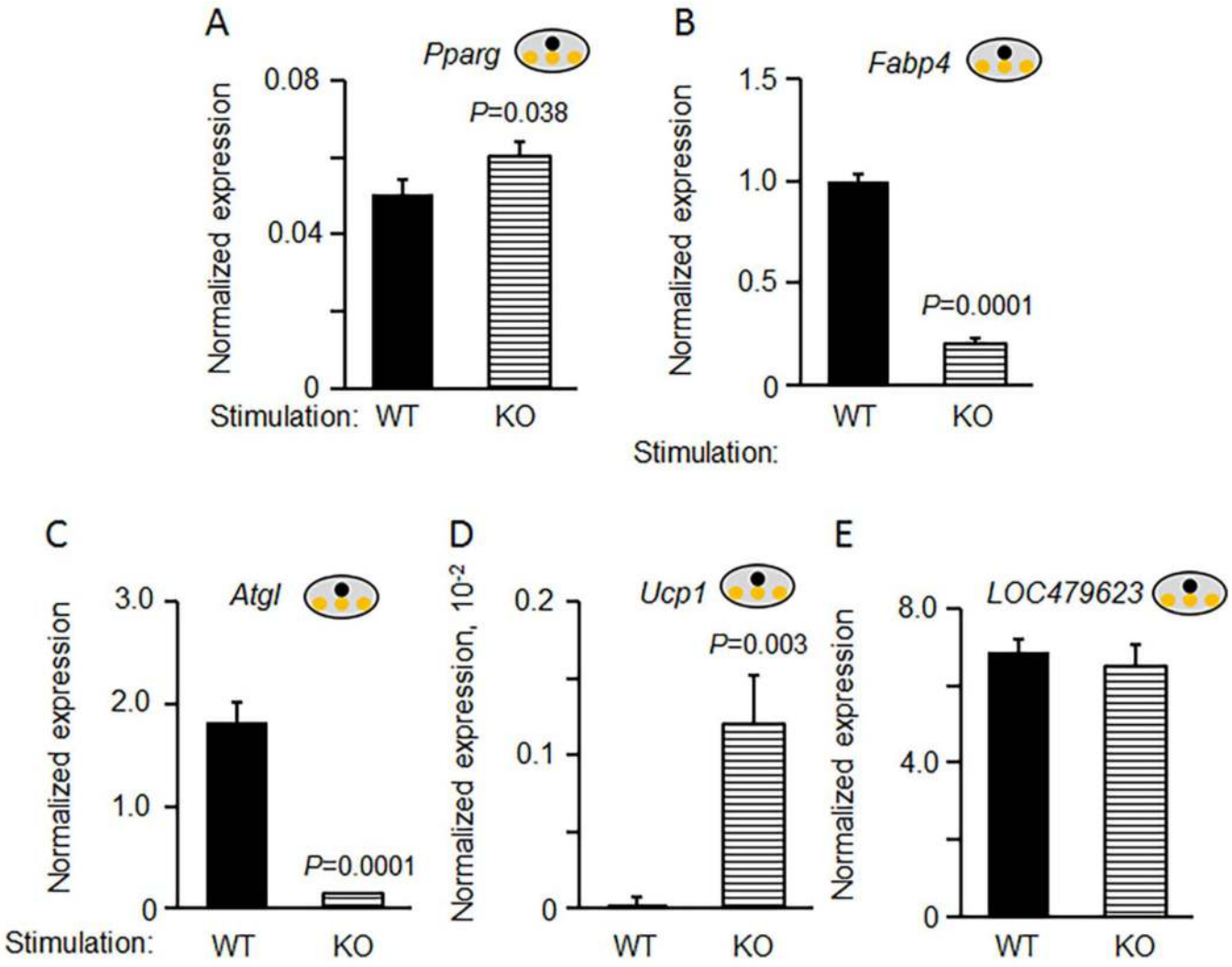

Figure 4. Co-culture of encapsulated murine WT and KO preadipocytes influence expression of genes in canine adipocytes isolated from a German Shepherd dog

Canine preadipocytes were differentiated in adipogenic medium with encapsulated WT or KO preadipocytes for 14 days (A-E). Expression of *Pparg* (A), *Fabp4* (B), *Atgl* (C), *Ucp1* (D) and *LOC479623* (E) were measured by Q-PCR assay TaqMan. The values were normalized by TBP and represent the mean ± SD (n=3), one-way ANOVA.

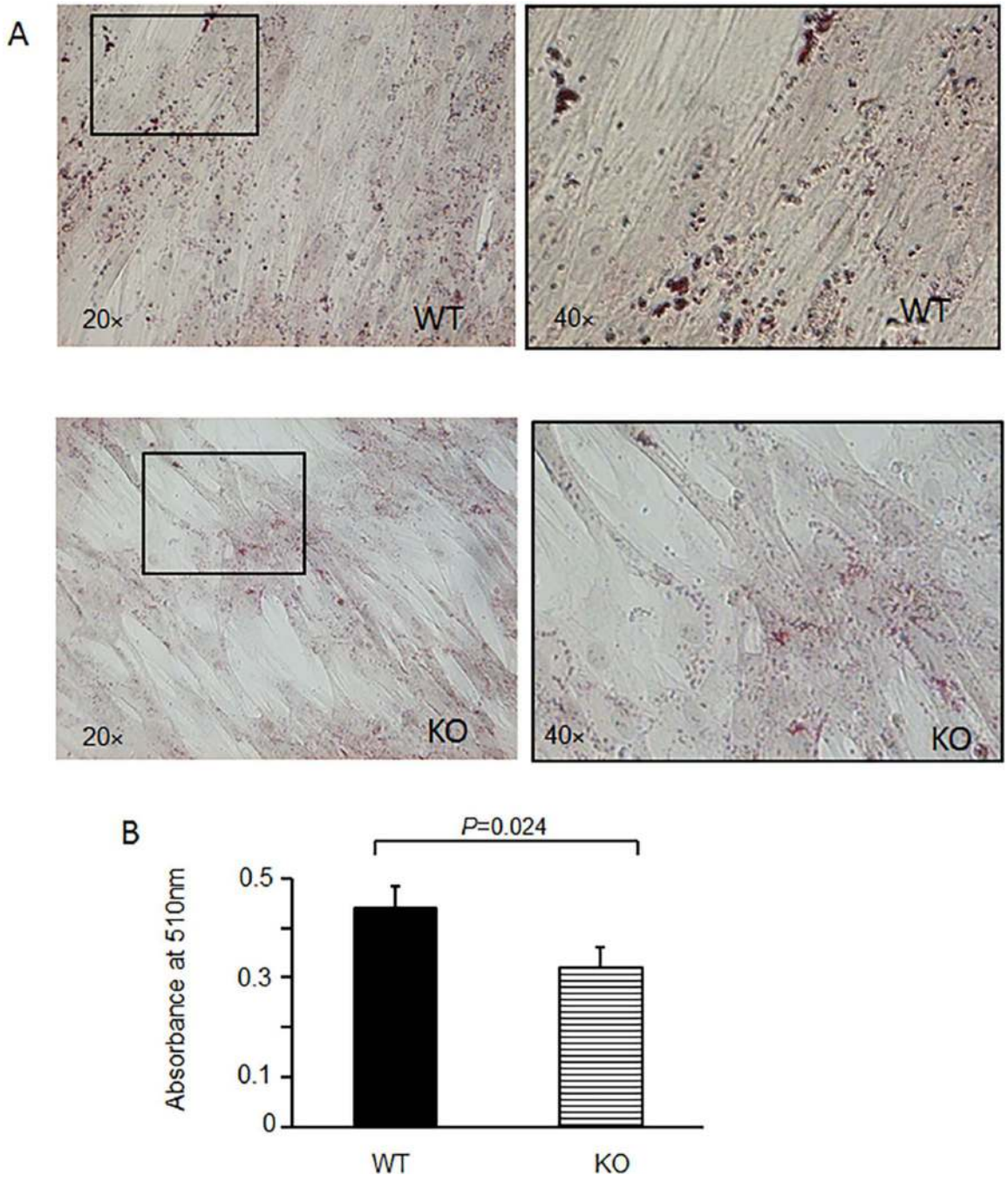

Figure 5. Encapsulated KO cells reduce lipid accumulation in canine adipocytes from a German Shepherd dog

Canine preadipocytes (German shepherd) were differentiated in adipogenic medium with encapsulated WT (upper panel in A, black bar in B) or KO preadipocytes (lower panel in A, patterned bars in B) for 14 days. Encapsulated WT and KO cells were removed. Neutral lipid accumulation in lipid droplet is shown in differentiated canine adipocytes using Oil Red O staining (A). Left panels showed enlarged (40x magnification) areas (square) in the right panels A. Lipid accumulation was quantified in isopropanol extract from these Oil red

O stained canine adipocytes by detecting absorbance of dissolved oil red staining at 510nm (B). Data are shown as mean ± SD (n=3), one-way ANOVA.

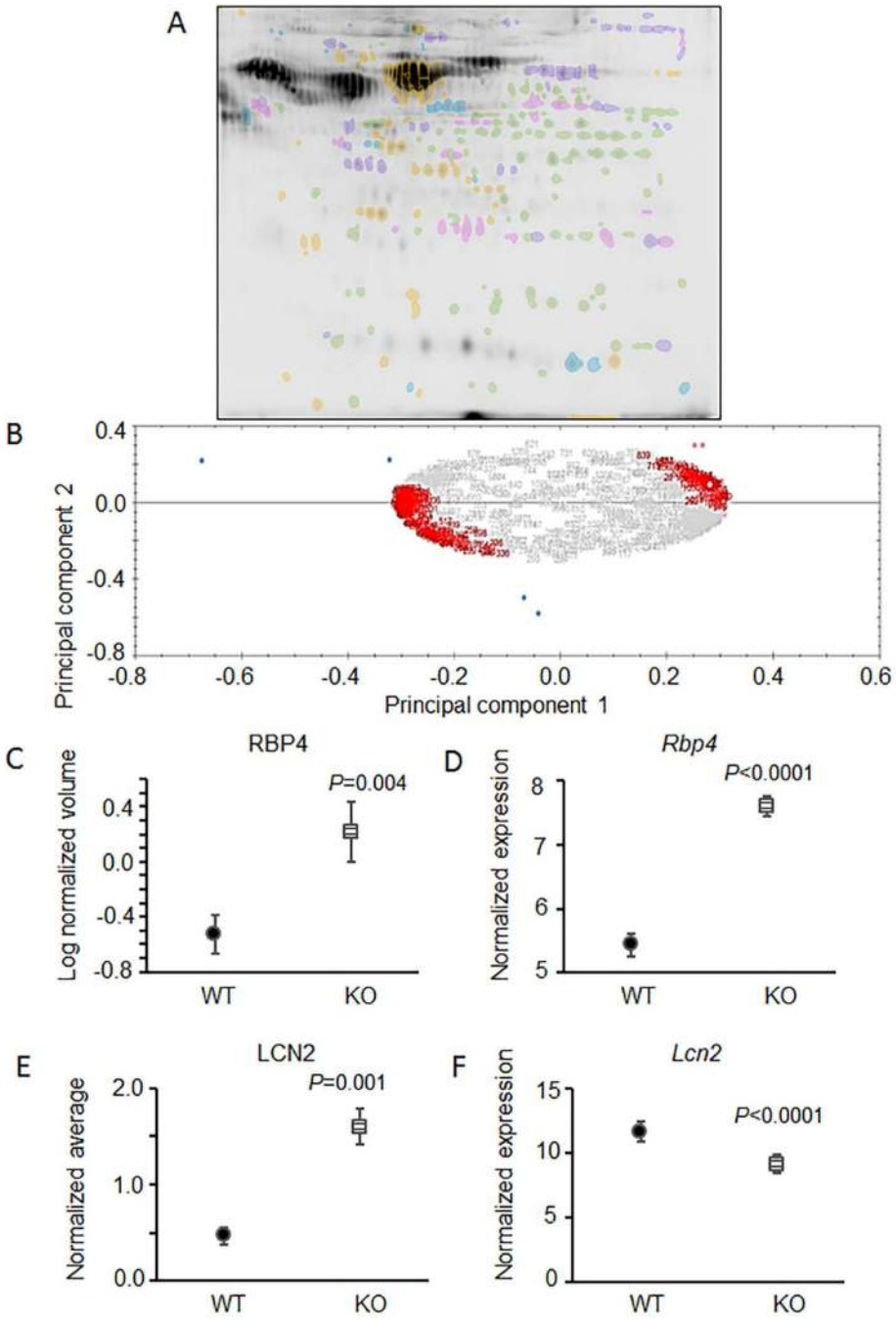

Figure 6. KO adipocytes secret higher levels of lipocalins RBP4 and LCN2 than WT adipocytes

DIGE was performed to identify different proteins (<50 kD) in the secretome from differentiated WT and from KO adipocytes (n=3 per condition). A representative 2D gel with protein spots that significantly changed by at least 1.5-fold (A). Principal component analysis (PCA) grouped of all proteins according to their similarity of standardized expression to determine how much variability between the proteins from WT and KO secretome (grey identification numbers, ID) (B). Red ID numbers showed secreted proteins that significantly changed by at least 1.5-fold between WT and KO secretome. Among

standardized expression profiles, the high variability protein clusters were identified in WT (pink dots) and KO (blue dot) secretomes. There were 2 major clusters of proteins exhibiting KO-induced downregulation and 3 major clusters of proteins exhibiting KO-induced upregulation. RBP4 protein abundance in secretomes from WT (black circle) and KO mouse adipocytes (white square) (C). Different *Rbp4* expression in WT and KO preadipocytes measured using Affymetrix GeneChip Mouse Gene ST 2.0 arrays (GEO file: 'QS wild type and Aldh1a1 KO preadipocytes 2015', n=3) (D). RBP4 protein abundance in secretomes from WT (black circle) and KO mouse adipocytes (white square) (E). Different *Lcn2* expression in WT and KO preadipocytes measured using Affymetrix GeneChip Mouse Gene ST 2.0 arrays (F).

Table 1

Protein Expression Changes in Murine Culture Media (KO vs WT)

Proteomic analysis of secretome from WT and KO adipocytes was performed by DIGE. Data shows proteins that were different in abundance in KOvs WT secretome (P<0.05, Student's *t*-test, n=3)

Spot #	Acc #	Desc[a]	pI	Mass	S[b]	M[c]
178	K2C1_MOUSE	Keratin, type II cytoskeletal 1 OS=Mus musculus GN=Krt1 PE=1 SV=4	8.39	66079	170	3
223	K1C10_MOUSE	Keratin, type I cytoskeletal 10 OS=Mus musculus GN=Krt10 PE=1 SV=3	5.04	57906	196	2
227	HS90B_MOUSE	Heat shock protein HSP 90-beta OS=Mus musculus GN=Hsp90ab1 PE=1 SV=3	4.97	83571	840	15
229		No ID				
233	HS90B_MOUSE	Heat shock protein HSP 90-beta OS=Mus musculus GN=Hsp90ab1 PE=1 SV=3	4.97	83571	711	11
	QSOX1_MOUSE	Sulfhydryl oxidase 1 OS=Mus musculus GN=Qsox1 PE=1 SV=1	6.73	83531	260	5
235	K2C1_MOUSE	Keratin, type II cytoskeletal 1 OS=Mus musculus GN=Krt1 PE=1 SV=4	8.39	66079	229	4
241	MYH4_MOUSE	Myosin-4 OS=Mus musculus GN=Myh4 PE=1 SV=1	5.58	223632	43	1
265	KV2A4_MOUSE	Ig kappa chain V-II region 2S1.3 OS=Mus musculus PE=1 SV=1	7.94	12327	102	1
271	CO6A1_MOUSE	Collagen alpha-1(VI) chain OS=Mus musculus GN=Col6a1 PE=2 SV=1	5.2	109562	56	1
282	PROS_MOUSE	Vitamin K-dependent protein S OS=Mus musculus GN=Pros1 PE=2 SV=1	5.61	76939	47	1
364	HS90B_MOUSE	Heat shock protein HSP 90-beta OS=Mus musculus GN=Hsp90ab1 PE=1 SV=3	4.97	83571	712	12
	K1C10_MOUSE	Keratin, type I cytoskeletal 10 OS=Mus musculus GN=Krt10 PE=1 SV=3	5.04	57906	374	6
	PDIA4_MOUSE	Protein disulfide-isomerase A4 OS=Mus musculus GN=Pdia4 PE=1 SV=3	5.16	72280	256	4
512	MYH4_MOUSE	Myosin-4 OS=Mus musculus GN=Myh4 PE=1 SV=1	5.58	223632	55	1
550	MYH4_MOUSE	Myosin-4 OS=Mus musculus GN=Myh4 PE=1 SV=1	5.58	223632	43	1
563		No ID				

Spot #	Acc #	Desc[a]	pI	Mass	S[b]	M[c]
597	PCOC1_MOUSE	Procollagen C-endopeptidase enhancer 1 OS=Mus musculus GN=Pcolce PE=1 SV=2	8.73	50820	367	6
601		No ID				
603	RD23A_MOUSE	UV excision repair protein RAD23 homolog A OS=Mus musculus GN=Rad23a PE=1 SV=2	4.56	39739	53	1
608	FSTL1_MOUSE	Follistatin-related protein 1 OS=Mus musculus GN=Fstl1 PE=1 SV=2	5.58	35672	182	3
	CO1A1_MOUSE	Collagen alpha-1(I) chain OS=Mus musculus GN=Col1a1 PE=1 SV=4	5.65	138974	107	2
	RINI_MOUSE	Ribonuclease inhibitor OS=Mus musculus GN=Rnh1 PE=1 SV=1	4.69	51495	103	2
628	PDIA6_MOUSE	Protein disulfide-isomerase A6 OS=Mus musculus GN=Pdia6 PE=1 SV=3	5	48469	785	12
647	FETUA_MOUSE		6.04	38100	52	1
657	ENOA_MOUSE	Alpha-enolase OS=Mus musculus GN=Eno1 PE=1 SV=3	6.37	47453	1160	17
669	NSF1C_MOUSE	NSFL1 cofactor p47 OS=Mus musculus GN=Nsfl1c PE=1 SV=1	5.04	40685	486	8
	TXND5_MOUSE	Thioredoxin domain-containing protein 5 OS=Mus musculus GN=Txndc5 PE=1 SV=2	5.51	47070	408	6
672	SPRC_MOUSE	SPARC OS=Mus musculus GN=Sparc PE=1 SV=1	4.77	35283	268	4
676	MYH4_MOUSE	Myosin-4 OS=Mus musculus GN=Myh4 PE=1 SV=1	5.58	223632	47	1
689	CO1A1_MOUSE	Collagen alpha-1(I) chain OS=Mus musculus GN=Col1a1 PE=1 SV=4	5.65	138974	68	1
706	PGK1_MOUSE	Phosphoglycerate kinase 1 OS=Mus musculus GN=Pgk1 PE=1 SV=4	8.02	44921	667	10
724	PGK1_MOUSE	Phosphoglycerate kinase 1 OS=Mus musculus GN=Pgk1 PE=1 SV=4	8.02	44921	301	4
752	CATB_MOUSE	Cathepsin B OS=Mus musculus GN=Ctsb PE=1 SV=2	5.57	38168	233	4
	K2C1_MOUSE	Keratin, type II cytoskeletal 1 OS=Mus musculus GN=Krt1 PE=1 SV=4	8.39	66079	156	3
	SPON2_MOUSE	Spondin-2 OS=Mus musculus GN=Spon2 PE=1 SV=2	5.45	36398	94	2
753	SPRC_MOUSE	SPARC OS=Mus musculus GN=Sparc PE=1 SV=1	4.77	35283	448	7
761	SPRC_MOUSE	SPARC OS=Mus musculus GN=Sparc PE=1 SV=1	4.77	35283	363	6

Spot #	Acc #	Desc[a]	pI	Mass	S[b]	M[c]
770	K2C1_MOUSE	Keratin, type II cytoskeletal 1 OS=Mus musculus GN=Krt1 PE=1 SV=4	8.39	66079	159	3
772	AATM_MOUSE	Aspartate aminotransferase, mitochondrial OS=Mus musculus GN=Got2 PE=1 SV=1	9.13	47780	450	7
781	GLRX3_MOUSE	Glutaredoxin-3 OS=Mus musculus GN=Glrx3 PE=1 SV=1	5.42	38039	377	6
783		No ID				
786	ILEUA_MOUSE	Leukocyte elastase inhibitor A OS=Mus musculus GN=Serpinb1a PE=1 SV=1	5.85	42719	1019	16
	CATL1_MOUSE	Cathepsin L1 OS=Mus musculus GN=Ctsl PE=1 SV=2	6.37	38093	164	3
787	VCAM1_MOUSE	Vascular cell adhesion protein 1 OS=Mus musculus GN=Vcam1 PE=1 SV=1	5.21	82406	149	3
788	CH3L1_MOUSE	Chitinase-3-like protein 1 OS=Mus musculus GN=Chi3l1 PE=1 SV=3	8.74	44150	111	2
789	K1C10_MOUSE	Keratin, type I cytoskeletal 10 OS=Mus musculus GN=Krt10 PE=1 SV=3	5.04	57906	203	3
797	CH3L1_MOUSE	Chitinase-3-like protein 1 OS=Mus musculus GN=Chi3l1 PE=1 SV=3	8.74	44150	771	13
799	CH3L1_MOUSE	Chitinase-3-like protein 1 OS=Mus musculus GN=Chi3l1 PE=1 SV=3	8.74	44150	462	8
800	CH3L1_MOUSE	Chitinase-3-like protein 1 OS=Mus musculus GN=Chi3l1 PE=1 SV=3	8.74	44150	582	10
804	MYH4_MOUSE	Myosin-4 OS=Mus musculus GN=Myh4 PE=1 SV=1	5.58	223632	42	1
805	SPRC_MOUSE	SPARC OS=Mus musculus GN=Sparc PE=1 SV=1	4.77	35283	300	5
806	SPRC_MOUSE	SPARC OS=Mus musculus GN=Sparc PE=1 SV=1	4.77	35283	443	7
	F10A1_MOUSE	Hsc70-interacting protein OS=Mus musculus GN=St13 PE=1 SV=1	5.19	41801	120	2
807	CH3L1_MOUSE	Chitinase-3-like protein 1 OS=Mus musculus GN=Chi3l1 PE=1 SV=3	8.74	44150	313	5
808	CWC25_MOUSE	Pre-mRNA-splicing factor CWC25 homolog OS=Mus musculus GN=Cwc25 PE=2 SV=2	10.23	48839	43	1
809	ALBU_MOUSE	Serum albumin OS=Mus musculus GN=Alb PE=1 SV=3	5.75	70700	63	1
	SPON2_MOUSE	Spondin-2 OS=Mus musculus GN=Spon2 PE=1 SV=2	5.45	36398	59	1
814	SPRC_MOUSE	SPARC OS=Mus musculus GN=Sparc PE=1 SV=1	4.77	35283	68	1

Spot #	Acc #	Desc[a]	pI	Mass	S[b]	M[c]
815	SPRC_MOUSE	SPARC OS=Mus musculus GN=Sparc PE=1 SV=1	4.77	35283	498	9
820	SPON2_MOUSE	Spondin-2 OS=Mus musculus GN=Spon2 PE=1 SV=2	5.45	36398	224	4
822	K2C1_MOUSE	Keratin, type II cytoskeletal 1 OS=Mus musculus GN=Krt1 PE=1 SV=4	8.39	66079	213	4
825		No ID				
828	K2C75_MOUSE	Keratin, type II cytoskeletal 75 OS=Mus musculus GN=Krt75 PE=1 SV=1	8.46	59932	134	2
829	CO1A1_MOUSE	Collagen alpha-1(I) chain OS=Mus musculus GN=Col1a1 PE=1 SV=4	5.65	138974	59	1
830	ALBU_MOUSE	**Serum albumin OS=Mus musculus GN=Alb PE=1 SV=3**	5.75	70700	67	1
845		No ID				
857	G3P_MOUSE	Glyceraldehyde-3-phosphate dehydrogenase OS=Mus musculus GN=Gapdh PE=1 SV=2	8.44	36072	497	7
862	G3P_MOUSE	Glyceraldehyde-3-phosphate dehydrogenase OS=Mus musculus GN=Gapdh PE=1 SV=2	8.44	36072	469	7
877	CATL1_MOUSE	Cathepsin L1 OS=Mus musculus GN=Ctsl PE=1 SV=2	6.37	38093	584	9
	ENOA_MOUSE	Alpha-enolase OS=Mus musculus GN=Eno1 PE=1 SV=3	6.37	47453	222	4
878	K2C1_MOUSE	Keratin, type II cytoskeletal 1 OS=Mus musculus GN=Krt1 PE=1 SV=4	8.39	66079	162	3
880	MDHM_MOUSE	Malate dehydrogenase, mitochondrial OS=Mus musculus GN=Mdh2 PE=1 SV=3	8.93	36045	459	8
	ROA2_MOUSE	Heterogeneous nuclear ribonucleoproteins A2/B1 OS=Mus musculus GN=Hnrnpa2b1 PE=1 SV=2	8.97	37437	412	6
883	ROA1_MOUSE	Heterogeneous nuclear ribonucleoprotein A1 OS=Mus musculus GN=Hnrnpa1 PE=1 SV=2	9.27	34289	277	4
885	IGHG1_MOUSE	Ig gamma-1 chain C region secreted form OS=Mus musculus GN=Ighg1 PE=1 SV=1	7.23	36252	392	6
	CATL1_MOUSE	Cathepsin L1 OS=Mus musculus GN=Ctsl PE=1 SV=2	6.37	38093	236	4
896	IGHG1_MOUSE	Ig gamma-1 chain C region secreted form OS=Mus musculus GN=Ighg1 PE=1 SV=1	7.23	36252	283	5
	CATL1_MOUSE	Cathepsin L1 OS=Mus musculus GN=Ctsl PE=1 SV=2	6.37	38093	102	2

Spot #	Acc #	Desc[a]	pI	Mass	S[b]	M[c]
898	IBP4_MOUSE	Insulin-like growth factor-binding protein 4 OS=Mus musculus GN=Igfbp4 PE=2 SV=2	6.81	28929	201	4
	IGH1M_MOUSE	Ig gamma-1 chain C region, membrane-bound form OS=Mus musculus GN=Ighg1 PE=1 SV=2	6.02	44043	176	3
899	ROA1_MOUSE	Heterogeneous nuclear ribonucleoprotein A1 OS=Mus musculus GN=Hnrnpa1 PE=1 SV=2	9.27	34289	339	5
	IGH1M_MOUSE	Ig gamma-1 chain C region, membrane-bound form OS=Mus musculus GN=Ighg1 PE=1 SV=2	6.02	44043	118	2
902	IGH1M_MOUSE	Ig gamma-1 chain C region, membrane-bound form OS=Mus musculus GN=Ighg1 PE=1 SV=2	6.02	44043	103	2
904	ROA1_MOUSE	Heterogeneous nuclear ribonucleoprotein A1 OS=Mus musculus GN=Hnrnpa1 PE=1 SV=2	9.27	34289	249	3
906	IGH1M_MOUSE	Ig gamma-1 chain C region, membrane-bound form OS=Mus musculus GN=Ighg1 PE=1 SV=2	6.02	44043	47	1
907	IGH1M_MOUSE	Ig gamma-1 chain C region, membrane-bound form OS=Mus musculus GN=Ighg1 PE=1 SV=2	6.02	44043	50	1
915	IGH1M_MOUSE	Ig gamma-1 chain C region, membrane-bound form OS=Mus musculus GN=Ighg1 PE=1 SV=2	6.02	44043	52	1
	CLCA_MOUSE	Clathrin light chain A OS=Mus musculus GN=Clta PE=1 SV=2	4.5	25646	51	1
927	EFHD2_MOUSE	EF-hand domain-containing protein D2 OS=Mus musculus GN=Efhd2 PE=1 SV=1	5.01	26775	176	3
	CO1A1_MOUSE	Collagen alpha-1(I) chain OS=Mus musculus GN=Col1a1 PE=1 SV=4	5.65	138974	161	3
930	CO1A1_MOUSE	Collagen alpha-1(I) chain OS=Mus musculus GN=Col1a1 PE=1 SV=4	5.65	138974	463	8
	IGH1M_MOUSE	Ig gamma-1 chain C region, membrane-bound form OS=Mus musculus GN=Ighg1 PE=1 SV=2	6.02	44043	112	2
943	IBP4_MOUSE	Insulin-like growth factor-binding protein 4 OS=Mus musculus GN=Igfbp4 PE=2 SV=2	6.81	28929	303	6
950	IBP4_MOUSE	Insulin-like growth factor-binding protein 4 OS=Mus musculus GN=Igfbp4 PE=2 SV=2	6.81	28929	236	4
953	IBP7_MOUSE	Insulin-like growth factor-binding protein 7 OS=Mus musculus GN=Igfbp7 PE=2 SV=3	8.71	29977	485	8
962	IBP7_MOUSE	Insulin-like growth factor-binding protein 7 OS=Mus musculus GN=Igfbp7 PE=2 SV=3	8.71	29977	186	3

Spot #	Acc #	Desc[a]	pI	Mass	S[b]	M[c]
969	HSP7C_MOUSE	Heat shock cognate 71 kDa protein OS=Mus musculus GN=Hspa8 PE=1 SV=1	5.37	71055	184	3
971	K2C1_MOUSE	Keratin, type II cytoskeletal 1 OS=Mus musculus GN=Krt1 PE=1 SV=4	8.39	66079	203	4
	IBP4_MOUSE	Insulin-like growth factor-binding protein 4 OS=Mus musculus GN=Igfbp4 PE=2 SV=2	6.81	28929	95	2
974	CO1A1_MOUSE	Collagen alpha-1(I) chain OS=Mus musculus GN=Col1a1 PE=1 SV=4	5.65	138974	122	2
982	FHL1_MOUSE	Four and a half LIM domains protein 1 OS=Mus musculus GN=Fhl1 PE=1 SV=3	8.76	33806	58	1
986	FINC_MOUSE	Fibronectin OS=Mus musculus GN=Fn1 PE=1 SV=4	5.39	276017	73	1
987		No ID				
989		No ID				
1009		No ID				
1017	FINC_MOUSE	Fibronectin OS=Mus musculus GN=Fn1 PE=1 SV=4	5.39	276017	108	2
1019	FINC_MOUSE	Fibronectin OS=Mus musculus GN=Fn1 PE=1 SV=4	5.39	276017	79	1
1035	GDIR1_MOUSE	Rho GDP-dissociation inhibitor 1 OS=Mus musculus GN=Arhgdia PE=1 SV=3	5.12	23450	569	8
1036	GDIR1_MOUSE	Rho GDP-dissociation inhibitor 1 OS=Mus musculus GN=Arhgdia PE=1 SV=3	5.12	23450	558	8
1041	GDIR1_MOUSE	Rho GDP-dissociation inhibitor 1 OS=Mus musculus GN=Arhgdia PE=1 SV=3	5.12	23450	51	1
1044	GDIR2_MOUSE	Rho GDP-dissociation inhibitor 2 OS=Mus musculus GN=Arhgdib PE=1 SV=3	4.97	22894	518	8
1065	PGAM1_MOUSE	Phosphoglycerate mutase 1 OS=Mus musculus GN=Pgam1 PE=1 SV=3	6.67	28928	410	7
1073	LYOX_MOUSE	Protein-lysine 6-oxidase OS=Mus musculus GN=Lox PE=1 SV=1	8.73	47356	210	3
	PGAM1_MOUSE	Phosphoglycerate mutase 1 OS=Mus musculus GN=Pgam1 PE=1 SV=3	6.67	28928	112	2
1091	CCL2_MOUSE	C-C motif chemokine 2 OS=Mus musculus GN=Ccl2 PE=1 SV=1	9.81	16544	46	1
1098		No ID				
1125	TIMP2_MOUSE	Metalloproteinase inhibitor 2 OS=Mus musculus GN=Timp2 PE=1 SV=2	7.45	24996	407	7

Spot #	Acc #	Desc[a]	pI	Mass	S[b]	M[c]
1131	TIMP2_MOUSE	Metalloproteinase inhibitor 2 OS=Mus musculus GN=Timp2 PE=1 SV=2	7.45	24996	585	9
1132	TIMP2_MOUSE	Metalloproteinase inhibitor 2 OS=Mus musculus GN=Timp2 PE=1 SV=2	7.45	24996	493	8
1134	CCL2_MOUSE	C-C motif chemokine 2 OS=Mus musculus GN=Ccl2 PE=1 SV=1	9.81	16544	45	1
1139	NGAL_MOUSE	**Neutrophil gelatinase-associated lipocalin OS=Mus musculus GN=Lcn2 PE=1 SV=1**	8.96	23032	174	3
1142	NGAL_MOUSE	**Neutrophil gelatinase-associated lipocalin OS=Mus musculus GN=Lcn2 PE=1 SV=1**	8.96	23032	173	3
1143	PARK7_MOUSE	Protein DJ-1 OS=Mus musculus GN=Park7 PE=1 SV=1	6.32	20236	336	6
1155	CCL2_MOUSE	C-C motif chemokine 2 OS=Mus musculus GN=Ccl2 PE=1 SV=1	9.81	16544	57	1
1156		No ID				
1163	KCY_MOUSE	UMP-CMP kinase OS=Mus musculus GN=Cmpk1 PE=1 SV=1	5.68	22379	122	2
1165	PGBM_MOUSE	Basement membrane-specific heparan sulfate proteoglycan core protein OS=Mus musculus GN=Hspg2 PE=1 SV=1	5.88	407847	435	6
1167	RET4_MOUSE	**Retinol-binding protein 4 OS=Mus musculus GN=Rbp4 PE=2 SV=2**	5.69	23533	243	4
	NGAL_MOUSE	**Neutrophil gelatinase-associated lipocalin** OS=Mus musculus GN=**Lcn2** PE=1 SV=1	8.96	23032	113	2
1195	PPIB_MOUSE	Peptidyl-prolyl cis-trans isomerase B OS=Mus musculus GN=Ppib PE=1 SV=2	9.56	23699	54	1
1197		No ID				
1202	PP14B_MOUSE	Protein phosphatase 1 regulatory subunit 14B OS=Mus musculus GN=Ppp1r14b PE=1 SV=2	4.74	16061	49	1
1220	PPIB_MOUSE	Peptidyl-prolyl cis-trans isomerase B OS=Mus musculus GN=Ppib PE=1 SV=2	9.56	23699	548	9
1222		No ID				
1227		No ID				
1230	TAGL2_MOUSE	Transgelin-2 OS=Mus musculus GN=Tagln2 PE=1 SV=4	8.39	22552	168	3
1233		No ID				

Spot #	Acc #	Desc[a]	pI	Mass	S[b]	M[c]
1234	K2C1_MOUSE	Keratin, type II cytoskeletal 1 OS=Mus musculus GN=Krt1 PE=1 SV=4	8.39	66079	162	3
1236	MANF_MOUSE	Mesencephalic astrocyte-derived neurotrophic factor OS=Mus musculus GN=Manf PE=1 SV=1	8.34	20817	103	1
1238		No ID				
1250		No ID				
1284	RNAS4_MOUSE	Ribonuclease 4 OS=Mus musculus GN=Rnase4 PE=2 SV=1	9.18	17470	304	5
	CYTC_MOUSE	Cystatin-C OS=Mus musculus GN=Cst3 PE=2 SV=2	9.18	15749	130	2
	FLNC_MOUSE	Filamin-C OS=Mus musculus GN=Flnc PE=1 SV=3	5.63	293560	106	2
1287	CYTC_MOUSE	Cystatin-C OS=Mus musculus GN=Cst3 PE=2 SV=2	9.18	15749	358	5
	RNAS4_MOUSE	Ribonuclease 4 OS=Mus musculus GN=Rnase4 PE=2 SV=1	9.18	17470	288	5
1295	CYTC_MOUSE	Cystatin-C OS=Mus musculus GN=Cst3 PE=2 SV=2	9.18	15749	70	1
1298		No ID				
1300	IGKC_MOUSE	Ig kappa chain C region OS=Mus musculus PE=1 SV=1	5.23	11942	49	1
1341	NGAL_MOUSE	Neutrophil gelatinase-associated lipocalin OS=Mus musculus GN=Lcn2 PE=1 SV=1	8.96	23032	135	2
1346	COF1_MOUSE	Cofilin-1 OS=Mus musculus GN=Cfl1 PE=1 SV=3	8.22	18776	98	2
1377		No ID				
1378		No ID				
1380	EF1A2_MOUSE	Elongation factor 1-alpha 2 OS=Mus musculus GN=Eef1a2 PE=1 SV=1	9.11	50764	111	2
1381	PGK1_MOUSE	Phosphoglycerate kinase 1 OS=Mus musculus GN=Pgk1 PE=1 SV=4	8.02	44921	380	6
1383	PGK1_MOUSE	Phosphoglycerate kinase 1 OS=Mus musculus GN=Pgk1 PE=1 SV=4	8.02	44921	390	6
1385	PGK1_MOUSE	Phosphoglycerate kinase 1 OS=Mus musculus GN=Pgk1 PE=1 SV=4	8.02	44921	83	2

Spot #	Acc #	Desc[a]	pI	Mass	S[b]	M[c]
1389		No ID				
1390	F10A1_MOUSE	Hsc70-interacting protein OS=Mus musculus GN=St13 PE=1 SV=1	5.19	41801	111	2
1391		No ID				
1393		No ID				
1394	AK1A1_MOUSE	Alcohol dehydrogenase [NADP(+)] OS=Mus musculus GN=Akr1a1 PE=1 SV=3	6.9	36792	149	2
1395		No ID				
1398	ROA1_MOUSE	Heterogeneous nuclear ribonucleoprotein A1 OS=Mus musculus GN=Hnrnpa1 PE=1 SV=2	9.27	34289	164	2
1401		No ID				
1402		No ID				
1406	K2C75_MOUSE	Keratin, type II cytoskeletal 75 OS=Mus musculus GN=Krt75 PE=1 SV=1	8.46	59932	152	2
1407	HSP7C_MOUSE	Heat shock cognate 71 kDa protein OS=Mus musculus GN=Hspa8 PE=1 SV=1	5.37	71055	62	1
1408	K22O_MOUSE	Keratin, type II cytoskeletal 2 oral OS=Mus musculus GN=Krt76 PE=2 SV=1	8.68	63319	97	2
1409	PRDX6_MOUSE	Peroxiredoxin-6 OS=Mus musculus GN=Prdx6 PE=1 SV=3	5.71	24969	156	3
	GRB2_MOUSE	Growth factor receptor-bound protein 2 OS=Mus musculus GN=Grb2 PE=1 SV=1	5.89	25336	143	2
1410		No ID				
1412	GDIR1_MOUSE	Rho GDP-dissociation inhibitor 1 OS=Mus musculus GN=Arhgdia PE=1 SV=3	5.12	23450	92	2
1413	CYTC_MOUSE	Cystatin-C OS=Mus musculus GN=Cst3 PE=2 SV=2	9.18	15749	130	2
1415	UB2L3_MOUSE	Ubiquitin-conjugating enzyme E2 L3 OS=Mus musculus GN=Ube2l3 PE=2 SV=1	8.68	18021	265	4
	CYTC_MOUSE	Cystatin-C OS=Mus musculus GN=Cst3 PE=2 SV=2	9.18	15749	136	2
1416		No ID				
1418	NGAL_MOUSE	**Neutrophil gelatinase-associated lipocalin OS=Mus musculus GN=Lcn2 PE=1 SV=1**	8.96	23032	64	1

Spot #	Acc #	Desc[a]	pI	Mass	S[b]	M[c]
1420	TAGL2_MOUSE	Transgelin-2 OS=Mus musculus GN=Tagln2 PE=1 SV=4	8.39	22552	59	1
1423	CYTC_MOUSE	Cystatin-C OS=Mus musculus GN=Cst3 PE=2 SV=2	9.18	15749	128	2
1424		No ID				
1425	K1C10_MOUSE	Keratin, type I cytoskeletal 10 OS=Mus musculus GN=Krt10 PE=1 SV=3	5.04	57906	80	1

[a]The following abbreviations and their meaning are used in the protein description: OS = Organism species, GN = gene name, PE = evidence for protein existence (1 = protein level evidence and 2 = transcript level evidence), SV = sequence version.

[b]The protein score is derived from Mascot and provides an indication of how well the peptides matched the indicated protein sequence. The actual score is calculated by the following equation: protein score = -10*Log(P), where P is the probability that the protein match is a random event. Scores above 100 indicate that $p < 0.05$.

[c]The protein match score indicates the number of unique peptides that matched the sequence of the identified protein. Two unique peptide matches to a protein sequence confirms the identity of a protein.